ELSEVIER

Object-based modeling of SOFC system: dynamic behavior of micro-tube SOFC

Tomoyuki Ota[a,*], Michihisa Koyama[a], Ching-ju Wen[a],
Koichi Yamada[b], Hiroshi Takahashi[a]

[a]*Department of Chemical System Engineering, The University of Tokyo, 7-3-1 Hongo, Bunkyo-ku, Tokyo 113-8656, Japan*
[b]*Department of Fine Materials Engineering, Shinshu University, 3-15-1 Tokida, Ueda, Nagano 386-8567, Japan*

Abstract

A simulation model for a tubular solid oxide fuel cell (SOFC) was developed by the object-based approach to calculate the current distribution, gas concentration distribution, and temperature distribution at the steady states and transient operation states. The transient electrical and temperature response to a load change was simulated for the both cells with the diameter of 22 mm (standard cell) and the diameter of 2.4 mm (micro-tube cell). The time required to reach the new steady state as the operating voltage was changed from 0.7 to 0.5 V for the micro-tube cell was found to be 15 s, which is much shorter than that of the standard cell.
© 2003 Elsevier Science B.V. All rights reserved.

Keywords: SOFC; Modeling; Object-based; Transient characteristics

1. Introduction

Solid oxide fuel cell (SOFC) has many advantages due to its high operation temperature, such as high energy conversion efficiency, flexibility of usable fuel type, and high temperature exhaust gas. However, the rapid start-up of SOFC is difficult due to its high operation temperature, so a good promise of the SOFC system as a stationary power supply system was mainly surveyed [1,2]. Recently, it is proved that SOFC with micro-tube cell having diameters of 2 mm could be heated up to operation temperature within a few seconds without any crack [3]. Further, micro-tube cells can reduce the system volume and therefore increase the output power density, because the effective electrode area per unit volume increases by decreasing the cell diameter. The higher output power density, in conjunction with the high tolerance to thermal stress makes it possible to apply SOFC systems as the power supply to vehicles [4,5].

During the operation of an SOFC system, the suppression of mechanical stress and the quick system response to a demand change are important. Mechanical stress, which leads to the mechanical breakdown of the cell components, can be classified into two types, i.e. residual thermal stress through fabrication and thermal stress caused by the tem-

perature distribution along the cell. In order to design the cell and stack, which can prevent the mechanical breakdown, the analysis of the temperature distribution is first necessary. Further, to apply SOFC systems to vehicles, it is important to investigate the transient characteristics of the SOFC.

Although such analyses by experimental approach are necessary, it is time consuming to investigate the characteristics for all the cells at various operating conditions only by experimental approach to optimize the system design. Computational modeling is an effective tool for designing the optimal SOFC system and for predicting their characteristics at the steady states and transient operating states. The transient electrical response of a planar cell [6] and a tubular cell [7,8] has been studied using the conventional cell component materials. However, we are not aware of any previous literature reporting the transient characteristics of SOFC for different cell and stack configurations and cell component materials on the same basis.

While there is a strong need to compare SOFC with different cell configuration and different cell components, an analysis and designing of the SOFC system requires interdisciplinary collaborations. An object-based modeling approach can work effectively for the interdisciplinary collaboration [9]. In an object-based model framework, each component model is modularized as an object with explicit interface. By defining the interfaces explicitly, each modeler only needs to assure that the interface of his or her own

---

* Corresponding author.

Nomenclature

Lists of symbols

C	concentration (mol m^{-3})
C_p	heat capacity: solid (J kg^{-1} K^{-1}); gas (J mol^{-1} K^{-1})
D	diffusion coefficient (m^2 s^{-1})
E	activation energy (J mol^{-1})
emf	electromotive force (V)
f	view factor (–)
F	Faraday constant (=96485 C mol^{-1})
h	heat transfer coefficient (W m^{-2} s^{-1})
$H_m(T)$	enthalpy of gas species m at T (J mol^{-1})
$H_m^0(T)$	heat formation of gas species m at T (J mol^{-1})
i	current density (A m^{-2})
J_m	molar flow rate of constituent m (mol s^{-1})
k	thermal conductivity (W m^{-1} K^{-1})
M	molecular mass (kg mol^{-1})
p	pressure (Pa)
p_o	total pressure (Pa)
q	heat (W)
$\bar{r}$	mean pore radius (m)
R	gas constant (=8.314 J mol^{-1} K^{-1})
S	surface area (m^2)
t	time (s)
T	temperature (K)
V	volume (m^3)

Greek symbols

δx	width of each sliced cell (m)
ε	porosity (–)
γ	proportionality constant for exchange current density (A m^{-2})
η	overpotential (V)
λ	emissivity (–)
ρ	density (kg m^{-3})
σ	Stefan–Boltzmann constant (W m^{-2} K^{-4})
ζ	tortuosity (–)
ϑ	transfer coefficient (–)

Indices

a	anode
act	activation
at	air feed tube
c	cathode
conc	concentration
cond	conduction
conv	convection
e	electrolyte
fuel	fuel
g	gas (fuel, oxidant)
gen	heat generation by entropy change
H$_2$	hydrogen
H$_2$O	water vapor
ox	oxidant
O$_2$	oxygen
rad	radiation
react	enthalpy gain due to mass transfer
s	solid (cell, air feed tube)
s–g	interface between solid and gas

model matches the interface of the framework instead of understanding all the implementation details of other models. This enhances the flexibility of model extension and makes it easy to replace models, which compose the model framework, with other models such as more precise models or models that is based on the different assumptions. As a first step to model SOFC system in an object-based approach, we have developed a simulation model that simulates the characteristics of a single tubular SOFC. By using the developed model, time responses of cells and transient temperature distribution profiles for both the standard tubular cell and micro-tube cell are compared in this study.

2. Model description

2.1. Cell configuration

Fig. 1 illustrates the configuration of the cathode-supported type tubular cell. $Zr_{0.84}Y_{0.16}O_{2-\delta}$ (YSZ), Ni-YSZ cermet, $La_{0.81}Sr_{0.09}MnO_{3-\delta}$ (LSM), and $La_{0.9}Sr_{0.1}CrO_{3-\delta}$ (LSCr) was used for electrolyte, anode, cathode, and interconnect, respectively. Although it is not explicitly shown in Fig. 1, Ni felt was used for the electrical contact between cells. The physical properties of each component material and gas are shown in Tables 1 and 2 [10–13]. We assumed that resistivites follow the Arrhenius equation. Because the molar specific heat of LSM was not found, we set the value as 100 J mol^{-1} K^{-1} in the calculation. In this study, we evaluated characteristics of SOFCs with two different dimensions. One is the cell with the diameter of 22 mm
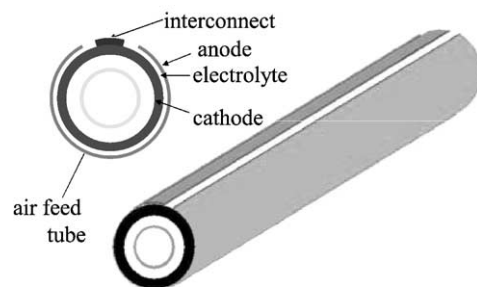

Fig. 1. Configuration of tubular SOFC.

Table 1
Physical properties of solid

Component	Anode	Electrolyte	Cathode	Interconnect	Air feed tube
Material	Ni-YSZ	YSZ	LSM	LSCr	Al_2O_3
Resistivity at 1073 K (Ω cm)	8.14×10^{-4}	45	0.014	3	–
Activation energy for resistivity (kJ mol^{-1})	11.6	−76.2	−5.0	0.12	–
Density (g cm^{-3})	6.87	5.90	6.57	–	3.95
Molar specific heat (J mol^{-1} K^{-1})	52	73	100	–	120
Thermal conductivity (W m^{-1} K^{-1})	4	4	4	–	10.4

Table 2
Physical properties of gas

Component	Molar specific heat (J mol^{-1} K^{-1})	Thermal conductivity (W m^{-1} K^{-1})
Fuel	–	0.46
Oxidant	–	0.071
H_2	31	–
H_2O	43	–
O_2	35	–
N_2	33	–

(standard cell) [14], and the other is the cell with the diameter of 2.4 mm (micro-tube cell) [4]. The dimensions of each cell and each cell component are listed in Table 3.

2.2. Overview of the model framework

Numbers of phenomena, such as reaction, mass transfer and heat transfer, and physical properties influence the characteristics of SOFC system. We make many simplifications when we construct simulation models, because it is too unrealistic to construct a model that takes all the phenomena occurring in the system into consideration. In addition, some of the physical property data are sometimes not available. Therefore, it is important to develop a model framework that enables users to flexibly change assumptions, physical properties, and cell configuration. As a first step to develop a model framework that satisfies these requirements, we have developed a model, which simulates current and tem-

Table 3
Cell dimension for the standard cell and the micro-tube cell

	Standard cell	Micro-tube cell
Effective cell length	150 cm	25 cm
Outer diameter of the cell	22 mm	2.4 mm
Thickness of cathode	2 mm	130 μm
Thickness of anode	100 μm	50 μm
Thickness of elecytrolyte	40 μm	20 μm
Diameter of air feed tube	12 mm	1.4 mm
Thickness of air feed tube	2 mm	0.1 mm
Thickness of interconnect	40 μm	70 μm

perature distributions of a single tubular cell, in an object-based fashion. The schematic image of the framework is shown in Fig. 2. In this framework, models that express physical entities are constructed separately from models that simulate physical, chemical and electrochemical phenomena occurring in the system. Physical entity models manage the information on dimensions, microstructure of cells and their components, and physical properties of chemical substances. Phenomena simulation models implemented in this study are equivalent circuit model, thermal model and fluid model. Equivalent circuit model simulates the current flow and the voltage distribution in the cell using the structural information and the physical property data from the physical entity models at a given operating conditions. The simulated current flow distribution data are input to the fluid model and the gas concentration distribution data from the fluid model are input to the equivalent circuit model. The heat generation due to the current flow through the cell is calculated using current flow and voltage distribution data. Heat generation data and gas concentration distribution data are then input to the thermal model. The temperature distribution data from the thermal model are input to the equivalent circuit model.
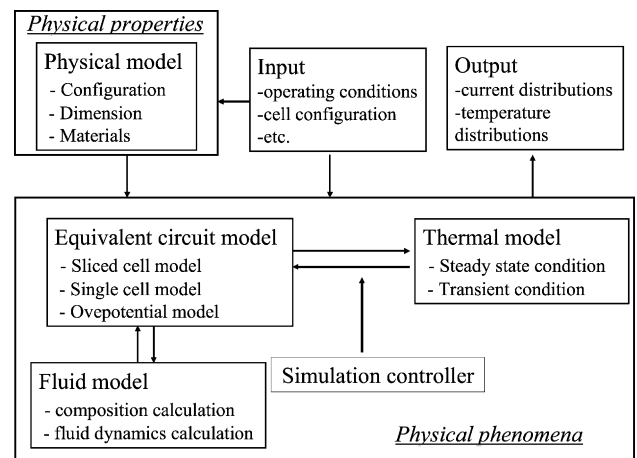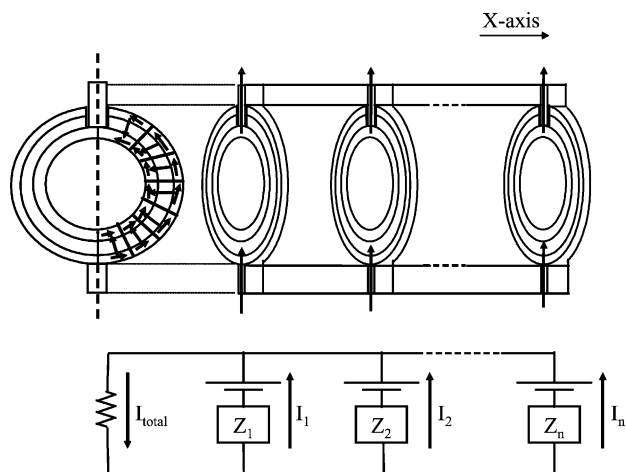

Fig. 2. Schematic image of the model framework.

Fig. 3. Equivalent circuit for sliced cell.

Fig. 4. Equivalent circuit for a cell mesh.

2.3. Phenomena simulation models

2.3.1. Equivalent circuit model

To simulate the electrochemical characteristics of the cell, we used the equivalent circuit as shown in Figs. 3 and 4. To simulate the tubular cell characteristics, the tubular cell was divided into slices by the planes perpendicular to X-axis, and denoted by ''sliced cell''. The sliced cell is divided concentrically into meshes, and they are denoted by ''cell mesh''. A sliced cell was modeled by a circuit composed of electromotive forces and cell impedances, Z. The cell characteristics are assumed to be symmetric with respect to the broken line shown in Fig. 3. The uniform electric potential along the X-axis was assumed for the electrical contact because the resistance of Ni felt is sufficiently low. Formulation details are described in Appendix A.

2.3.2. Fluid model

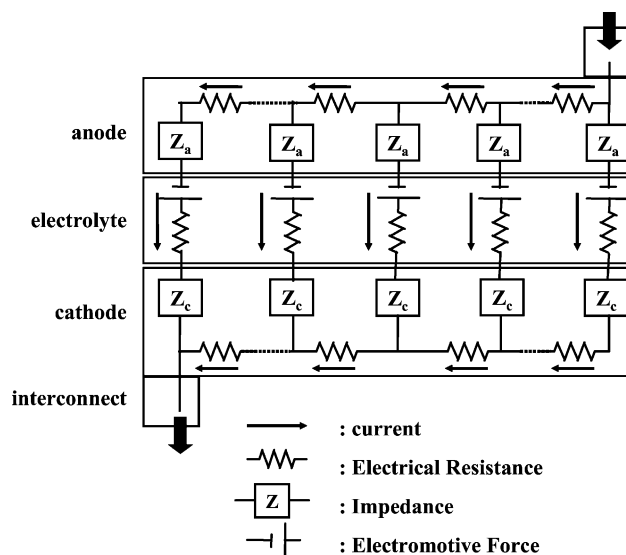Fluid model calculates flow rate and gas composition distributions at the given temperature and current flow distributions. For the calculation, fluid compartment is divided into slices in the exactly the same way with that for the cell. The slices in the anode compartment, cathode compartment, and air inlet tube compartment are denoted by fuel slice, oxidant slice, and inlet oxidant slice, respectively. The gas slice includes all the slices mentioned above. For simplification, the gas concentration is assumed to be uniform in each gas slice. Chemical species considered in this manuscript are H_2, O_2 and H_2O for fuel; O_2 and N_2 for oxidant. We assumed that all the gases are ideal and incompressible fluids. Faraday's law governs the change in constituents due to electrochemical reactions.

2.3.3. Thermal model

Heat transfer occurs through thermal conduction, convection and radiation. Fig. 5 shows the schematic image of heat transfer assumed in our model. The air feed tube is
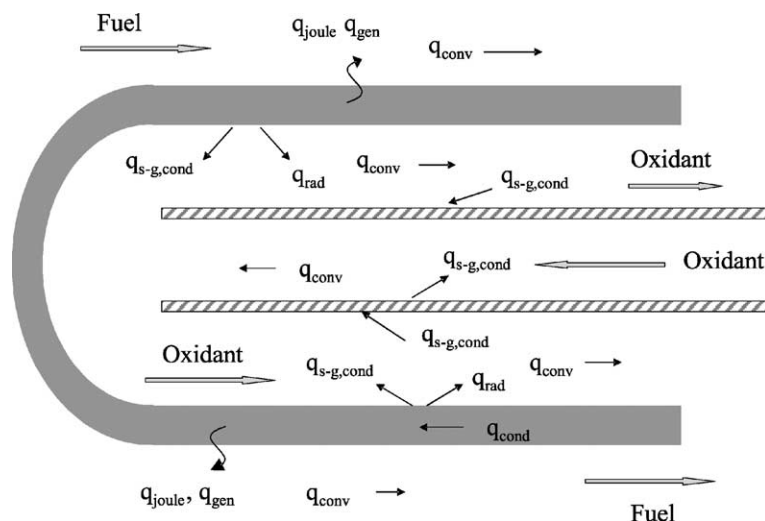

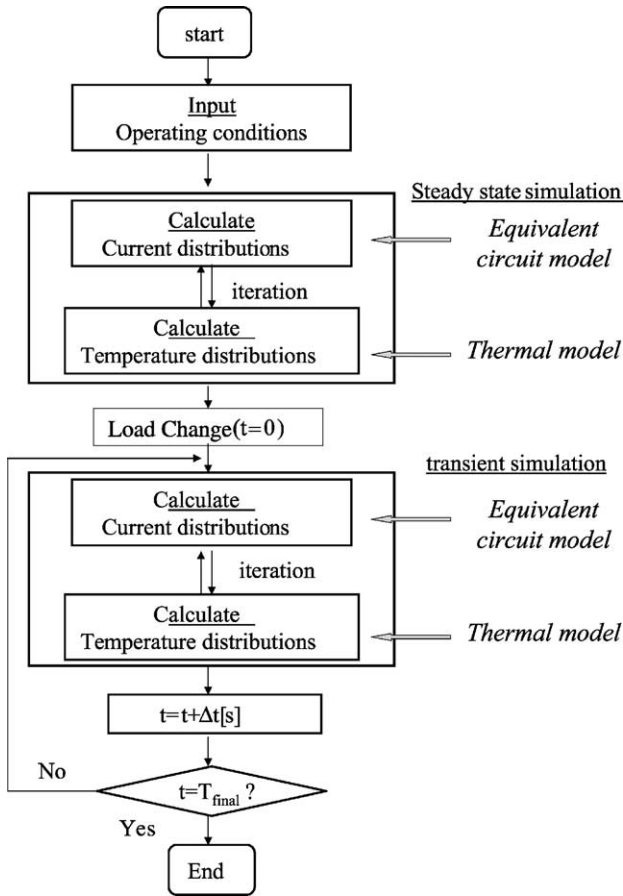Fig. 5. Schematic image of thermal transport phenomena.

Fig. 6. Schematic algorithm of transient simulation.

small compared with convection and heat conduction between gas and solid. Heat radiation was considered between cell and air feed tube but was not considered between cells. The heat exchange between solids and fluids due to heat radiation was also neglected [15]. Formulation details are described in Appendix B.

2.3.4. Simulation controller

The simulation controller controls both the equivalent circuit model and the thermal model to simulate current and temperature distributions. Fig. 6 shows a flow chart for the simulation process of the transient characteristics. In the transient phenomena, the rates of electrical, chemical and electrochemical processes were assumed to be sufficiently fast compared with those of thermal processes. First the distributions for the steady state condition at given operating condition is derived after iterating the input and output data exchange between phenomena simulation models. Then the cell voltage is suddenly changed to simulate the transient characteristics of the cell. Next the current and gas concentration distributions at $t = \Delta t$ are calculated using the new cell voltage and temperature distribution at $t = 0$. Using the obtained current and gas concentration distributions, temperature distribution is subsequently calculated. Thus, the transient characteristics of electrical response of the cell are determined stepwise.

3. Results and discussion

3.1. Steady state characteristics

The current and temperature distributions at the steady state were simulated for both the standard cell and the micro-tube cell. The operation conditions are listed in Table 4. In
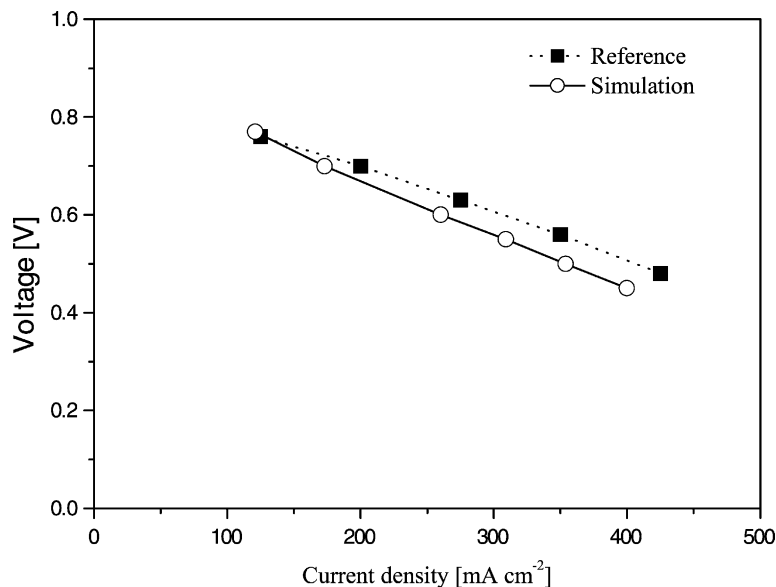
divided into slices by the same plane dividing the tubular cell into sliced cell. In this study, temperature of each sliced cell is assumed to be uniform. In addition, heat conduction between sliced cells was neglected because it is considerably

Fig. 7. I–V characteristics.

Table 4
Operation conditions for steady state simulation

Temperature (K)	1123
Pressure (MPa)	0.1
Fuel	97% H_2, 3% H_2O
Oxidant	Air (21% O_2, 79% N_2)
Fuel Utilization	0.80
Air Utilization	0.25

this study, temperatures of the inlet fuel and the oxidant at the closed end of the cell were assumed to be the same.

I–V characteristics of the standard cell are shown in Fig. 7. The temperature at the middle of the cell is defined as the operation temperature. *I–V* characteristics reported by Sin-

ghal [14] are also shown in Fig. 7 for reference. The simulated *I–V* characteristics for the standard cell at 890–960 °C show the similar tendency as that of the reported characteristics at 900 °C. However, the deviation between experimental data and simulation data indicates that the future revision of the electrical and electrochemical cell characteristics is necessary.

The current and temperature profiles along the *X*-axis for the cells are shown in Figs. 8 and 9. The left hand vertical axis is the amount of current that flow through the sliced cell. For both cells, the temperature increases and then decreases along the *X*-axis. In the micro-tube cell, the current increase along the flow direction as temperature increases, and decreases before the temperature decreases. On the other
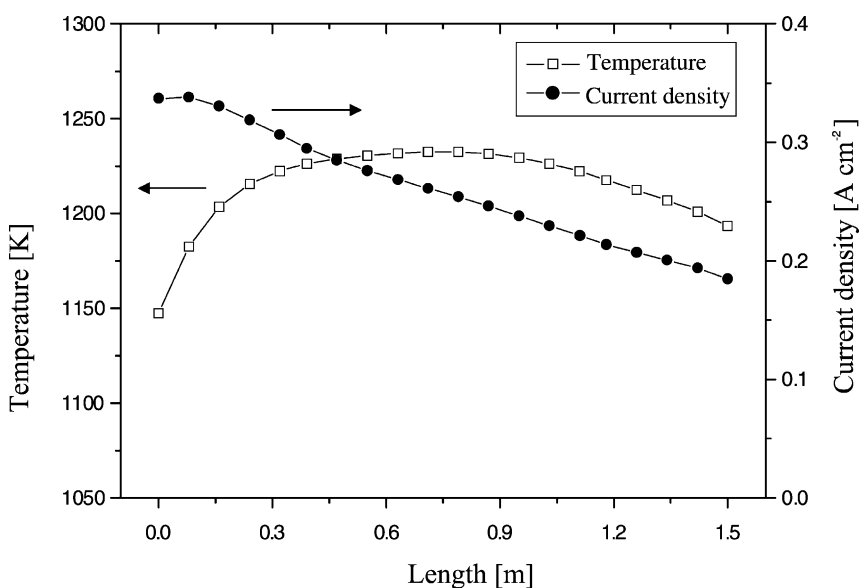

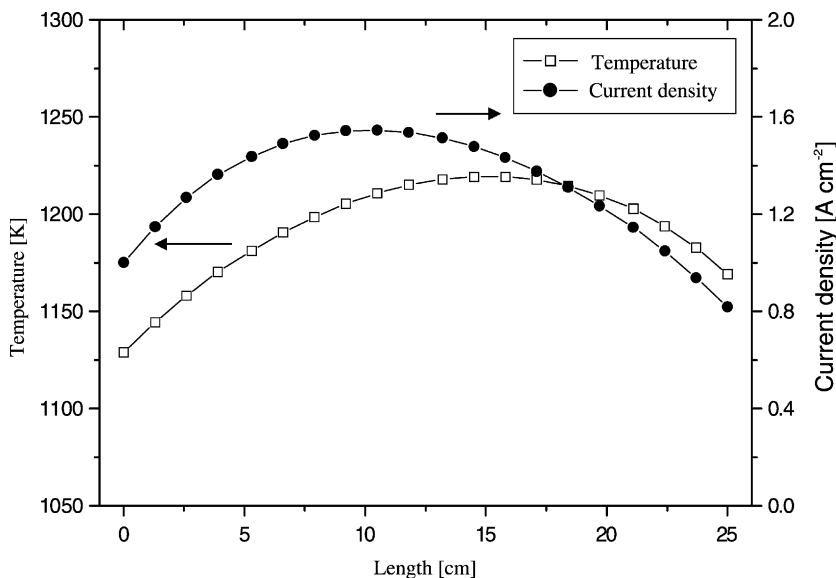Fig. 8. Current and temperature distributions at the steady state for the standard cell.

Fig. 9. Current and temperature distributions at the steady state for the micro-tube cell.
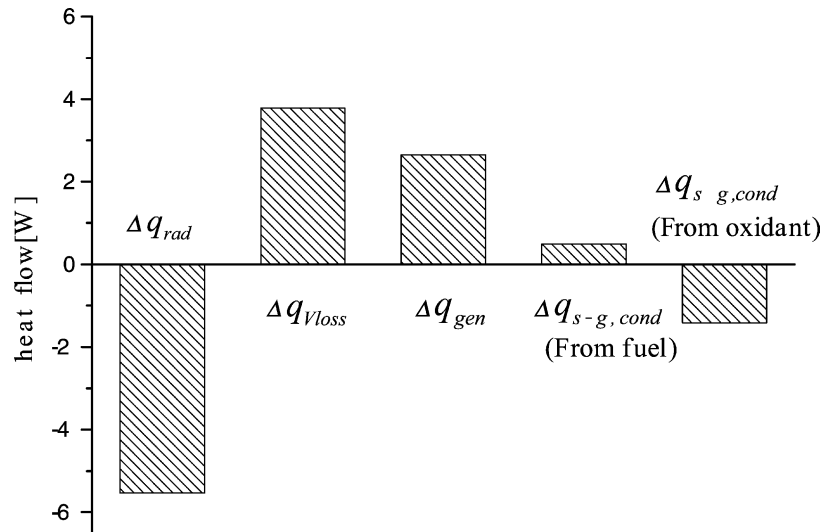
Fig. 10. Net heat gain by each type of heat transfer.

hand, in the standard cell, the current decreases along the *X*-axis in spite of temperature increase. This is because that the effect on V_{out} due to decrease of fuel concentration is larger than that due to the decrease of overpotential and ohmic loss as the temperature increases. The temperature difference between the maximum temperature and minimum temperature is almost same for both cells. Therefore, the temperature gradient per unit length is steeper in the micro-tube cell compared with that in the standard cell. However, Kendall and Palin [3] demonstrated that the micro-tube cell could generate power without any crack throughout the operation on the severe condition that the cell was directly heated by a butane burner. These results indicate that the stability of micro-tube cell is not due to the small temperature difference, but its resistance to stress. When the temperature gradient in the micro-tube cell causes some problems nevertheless of the reported results [3], the extension of the cell length will mitigate the problems.

The rates of each type of heat transfer for the sliced cell at the center of the standard cell are shown in Fig. 10. Using the obtained temperature profile for the standard cell, the rate of heat conduction between sliced cells was calculated. The calculated rate of heat conduction is less than 1% of the other types of heat flow rates shown in Fig. 10, which indicates that neglecting the heat conduction between sliced cells is reasonable in the simulation. Fig. 10 clearly shows that the rate of heat radiation from the cell to the air feed tube is considerably high. Consequently, it is important to take the heat radiation between cells into account in the future work.

3.2. Transient simulation

The transient electrical response and the temperature profile of each component were simulated as the terminal voltage drops from 0.7 to 0.5 V at $t = 0$. The flow rates of fuel and oxidant were kept constant in this simulation. In the practical SOFC system, fuel flow rates will be controlled to keep the utilization ratio constant corresponding to the load change. Therefore, the inlet gas temperatures will change because the inlet gases are preheated by using the heat from exhaust gas. The temperature of the exhaust gas will vary as the load changed, therefore, the temperature of fuel and oxidant after passing through the heat exchangers, will be different from that for the rated operation condition. However, inlet temperatures of fuel and oxidant were kept constant for simplification in the calculation.

Parameters for the simulation and the conditions for both cells before and after the cell voltage changed at $t = 0$ are listed in Table 5. Figs. 11 and 12 show the transient power profiles for the standard cell and the micro-tube cell, respectively. The time to reach the new steady state for the standard cell is 180 s, while 15 s for the micro-tube cell.

The transient response of the micro-tube cell is much quicker than that of the standard cell because the heat capacity of the micro-tube cell is smaller than that of the

Table 5
Initial and final conditions and parameters for transient simulation

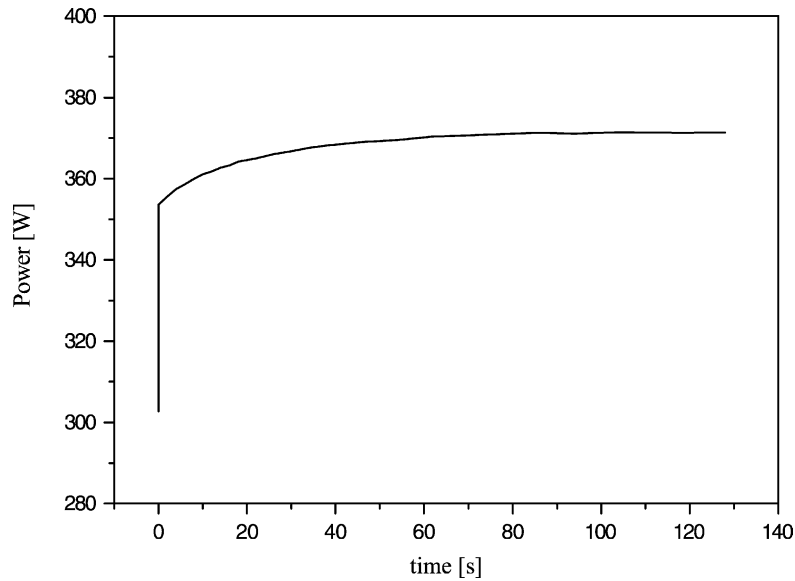|	Standard cell	Micro-tube cell
Input gas		
Fuel flow rate (mol s^{-1})	2.4×10^{-3}	3.2×10^{-4}
Oxidant flow rate (mol s^{-1})	1.5×10^{-2}	2.0×10^{-3}
Fuel inlet temperature (K)	1123	1123
Inlet Oxidant temperature (K)	1040	1098
Initial condition		
Fuel utilization	0.46	0.21
Air utilization	0.17	0.08
Current density (mA cm^{-2})	208	722
Power (W)	303	19
Final condition		
Fuel utilization	0.80	0.80
Air utilization	0.30	0.30
Current density (mA cm^{-2})	358	2.750
Power (W)	371	52

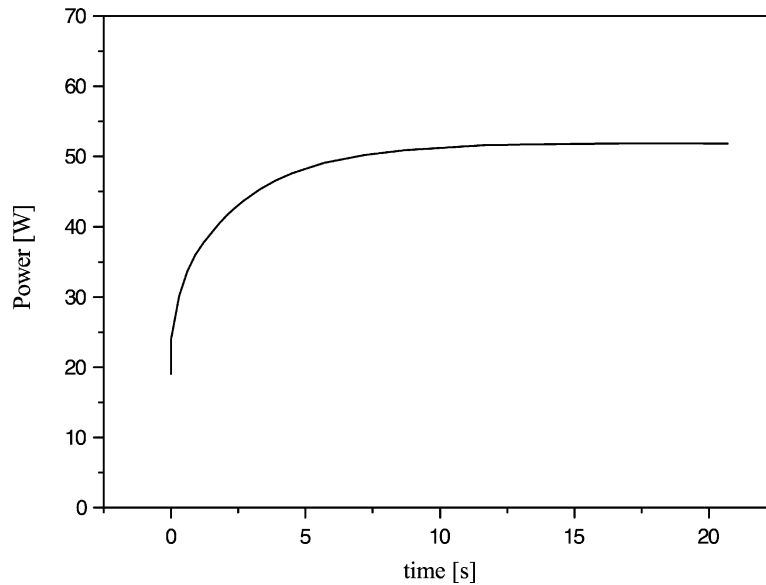Fig. 11. Time dependence of output power for the standard cell.

Fig. 12. Time dependence of output power for the micro-tube cell.

standard cell. The quick time response is preferable for the application of SOFC systems to the power supply for vehicles because it reduces the capacity of backup battery.

4. Conclusions

A model framework was developed in an object-based fashion to simulate the transient characteristics of tubular SOFC. Transient characteristics of tubular cells with the cell diameter of 22 and 2.4 mm were simulated. The results of steady state simulation show that the temperature gradient in the micro-tube cell is six times larger than that of the standard cell. On the other hand, the results of the transient

simulation show the quick response to a load change in the micro-tube cell. Because the quick response to a load change is essential in transportation application, the micro-tube cell demonstrated the possibility for transportation application.

Appendix A

The electromotive force of a cell, emf, is calculated by the Nernst equation:

$$\text{emf} = \frac{RT}{4F} \ln \frac{p_{O_2,c}}{p_{O_2,a}} \tag{A.1}$$

p_{O_2}, R, T, and F have usual meanings. The partial pressure of oxygen in anode was calculated assuming equilibrium condition in the gas phase.

The operating cell voltage, V_{out}, is expressed as follows:

$$V_{out} = emf - \eta_a - \eta_c - \eta_{IR} \quad (A.2)$$

η_a and η_c are the anodic and cathodic overpotentials, respectively, and η_{IR} is the ohmic loss at the electrolyte, the electrodes, and the interconnect. The operating cell voltage was calculated by using the equivalent circuit model considering the current distribution in the tubular cell.

Electrode overpotential is consist of activation overpotential, η_{act}, and concentration overpotential, η_{conc}.

$$\eta = \eta_{act} + \eta_{conc} \quad (A.3)$$

Eq. (A.4), given by Costamagna and Honegger [16], expresses the relationship between anodic activation overpotential, $\eta_{act,a}$, for Ni-YSZ anode and current density.

$$i = i_{0,a} \left\{ \exp\left(\vartheta_1 \frac{F}{RT} \eta_{act,a} \right) - \exp\left(\vartheta_2 \frac{F}{RT} \eta_{act,a} \right) \right\} \quad (A.4)$$

$i_{0,a}$ is the anodic exchange current density. Mogensen has proposed Eq. (A.5) for the anodic exchange current density [17,18].

$$i_{0,a} = \gamma_a \left(\frac{p_{H_2}}{p_{o,fuel}} \right) \left(\frac{p_{H_2O}}{p_{o,fuel}} \right) \exp\left(-\frac{E_a}{RT} \right) \quad (A.5)$$

The dependence of cathodic activation overpotential for LSM on current density was formulated based on experimental results by Fukunaga [19]:

$$\eta_{act,c} = 11 \times 10^6 \times \exp\left[\left(\frac{1}{T} - \frac{1}{1123} \right) \frac{E_c}{R} \right] \times i_c \quad (A.6)$$

E_c is the activation energy for cathodic activation overpotential and was assumed to be 200 kJ mol^{-1}.

The concentration overpotential is a potential drop caused by the concentration difference in the gas phase. In this study, we assumed that concentration gradient in the gas phase exists only in the porous electrodes.

Diffusion through the porous material is typically described by either or both of the binary molecular diffusion and Knudsen diffusion. In this study, both types of diffusion were taken into account to estimate the concentration overpotentials [20].

The binary molecular diffusion coefficient between gas species i and j in free space is estimated by the Chapman–Enskog theory [21]:

$$D_{ij} = 0.0018583 \left(\frac{1}{M_i} + \frac{1}{M_j} \right)^{1/2} \frac{T^{3/2}}{p\sigma_{ij}^2 \Omega_{ij}} \quad (A.7)$$

We note that the units for total pressure, p, is atm and σ is used to denote the collision diameter only for this

equation. The unit for collision diameter is Å. Ω_{ij} is the collision integral based on the Lennard–Jones potential.

Eq. (A.8) expresses the Knudsen diffusion coefficient for gas species i.

$$D_{ik} = 97.0\bar{r}\sqrt{\frac{T}{M_i}} \quad (A.8)$$

An effective diffusion coefficient considering both binary molecular diffusion and Knudsen diffusion was calculated as follows [20]:

$$\frac{1}{D_{i(eff)}} = \left(\frac{1}{D_{ij}} + \frac{1}{D_{ik}} \right) \left(\frac{\zeta}{\varepsilon} \right) \quad (A.9)$$

Tortuous path through the electrode microstructure was taken into account by tortuosity, ζ, and porosity, ε.

Appendix B. Enthalpy balance equations

The enthalpy balance equation can be described as follows.

$$\rho C_p \Delta V \frac{dT}{dt} = q_{total} \quad (B.1)$$

ρ and C_p are density and molar heat capacity, respectively. ΔV is the control volume of each slice.

For the steady state, left hand term in Eq. (B.1) is eliminated.

In each gas slice, q_{total} can be expressed as Eq. (B.2).

$$q_{total} = \Delta q_{conv} + \Delta q_{cond} + \Delta q_{s-g,cond} + \Delta q_{react} \quad (B.2)$$

The net enthalpy gain by convection, Δq_{conv}, can be expressed as Eq. (B.3) using the heat flux by convection, q_{conv}, expressed as Eq. (B.4).

$$\Delta q_{conv} = q_{conv}(z) - q_{conv}(z - 1) \quad (B.3)$$

$$q_{conv}(z) = \sum_m J_m(z) H_m(T_g(z)) \quad (B.4)$$

J_m is the molar flow rate of species m, and H is the enthalpy expressed by Eq. (B.5).

$$H_m(T_g(z)) = H_m^0(T_0) + \int_{T_0}^{T_g(z)} C_{p,m} dT \quad (B.5)$$

The net heat gain by conduction, $\Delta q_{condction}$, can be expressed as

$$\Delta q_{cond} = \left[T_g(z+1) + T_g(z-1) - 2T_g(z) \right] \frac{k_g S_g}{\delta x} \quad (B.6)$$

S and k, respectively are the area and thermal conductivity.

The net heat gain by heat conduction between solid and gas, $\Delta q_{s-g,cond}$, can be expressed as

$$\Delta q_{s-g,cond} = \left[T_s(z) - T_g(z) \right] S_{s-g} h_g \quad (B.7)$$

The net enthalpy gain due to mass transfer into the electrode porous space, Δq_{react}, can be expressed as

$$\Delta q_{react} = -\frac{i_e}{4F} H_{O_2}(T_{ox}(z)) \quad \text{(for the oxidant)} \tag{B.8}$$

$$\Delta q_{react} = -\frac{i_e}{2F} [H_{H_2}(T_{fuel}(z)) - H_{H_2O}(T_{fuel}(z))] \quad \text{(for the fuel)} \tag{B.9}$$

i_e is the current density through the electrolyte.

In each solid slice:

$$q_{total} = \Delta q_{cond} + \Delta q_{Vloss} + \Delta q_{s-g,cond} + \Delta q_{rad} + \Delta q_{gen} \tag{B.10}$$

$\Delta q_{V,loss}$ is the heat generation due to voltage losses at the cell.

The heat generation term by entropy change through the electrode reactions, Δq_{gen}, can be expressed as

$$\Delta q_{gen} = -\frac{i_e}{2F} \Delta H_{H_2O}(T_s) - \text{emf}\, i_e \tag{B.11}$$

The net heat gain by radiation, Δq_{rad}, can be expressed as

$$\Delta q_{rad} = f\sigma\lambda(T_{cell}^4 - T_{at}^4) \tag{B.12}$$

Because the length of the fluid channel along the cell is sufficiently long compared with the distance between cell and air feed tube, only the vertical heat radiation between cell and air feed tube was only taken into account. Heat radiation is assumed between the air inlet tube and cell.

The heat transfer coefficient, h, can be expressed by Eq. (B.13) assuming a fully developed laminar flow at constant wall temperature, when the Reynolds number of fluid is less than 2100 [22].

$$\frac{hd}{k} = 3.66 \tag{B.13}$$

d is the equivalent diameter of the gas channel. The thermal conductivities of gases are taken from [23]. For simplification, the temperature dependence of thermal conductivity was not considered.

References

[1] A.J. Appleby, F.R. Foulkes, Fuel Cell Handbook, Nostrand Reinhold, New York, 1989.
[2] Y. Matsumoto, R. Yokoyama, K. Ito, J. Eng. Gas Turbines Power Trans. ASME 116 (1994) 8–14.
[3] K. Kendall, M. Palin, J. Power Sources 71 (1998) 268–279.
[4] K. Yamada, N. Takahashi, C. Wen, J. Chem. Eng. Jpn, in press.
[5] S.B. Kraines, D.R. Wallace, Y. Iwafune, Y. Yoshida, T. Aramaki, K. Kato, K. Hanaki, H. Ishitani, T. Matsuo, H. Takahashi, K. Yamada, K. Yamaji, Y. Yanagisawa, H. Komiyama, An integrated computational infrastructure for a virtual Tokyo: concepts and examples, J. Ind. Ecol. 5 (1) (2001) 35–54.
[6] E. Achenbach, J. Power Sources 49 (1994) 333–348.
[7] D.J. Hall, R.G. Colclaser, IEEE Trans. Energy Convers. 14 (1999) 749–753.
[8] C. Haynes, J. Power Sources 109 (2002) 365–376.
[9] J.V. Herle, R. Ihringer, N.M. Sammes, G. Tompsett, K. Kendall, K. Yamada, C. Wen, T. Kawada, M. Ihara, J. Mizusaki, Solid State Ionics 132 (2000) 333–342.
[10] N.F. Bessette II, W.J. Wepfer, J. Winnick, J. Electrochem. Soc. 142 (1995) 3792–3800.
[11] J. Kuroki, Y. Yamazaki, H. Watabe, T. Arakawa, in: Proceedings for the Ninth Symposium on Solid Oxide Fuel Cells in Japan, The Solid Oxide Fuel Cell Society of Japan, Japan, 2000, p. 34.
[12] N. Seki, Engineering of Heat Transfer, Morikita Publisher Inc., Tokyo, 1988, p. 242 (in Japanese).
[13] H. Tagawa, Solid Oxide Fuel Cell and Global Environment, Agune-Syoufu Inc., Tokyo, 1988 (in Japanese).
[14] S.C. Singhal, Solid State Ionics 135 (2000) 305–313.
[15] A. Hirano, M. Suzuki, M. Ippommatsu, J. Electrochem. Soc. 139 (1992) 2744–2751.
[16] P. Costamagna, K. Honegger, J. Electrochem. Soc. 145 (1998) 3995–4007.
[17] M. Mogensen, T. Lindegaard, in: Proceedings for the Third International Symposium on Solid Oxide Fuel Cells, PV 93-4, The Electrochemical Society Proceedings Series, Pennington, NJ, 1993, p. 484.
[18] M. Mogensen, in: Proceedings of the 14th Riso International Symposium on Material Science, Riso National Laboratory, Ros-kilde, Denmark, 1993, p. 117.
[19] H. Fukunaga, Ph.D. Thesis, The University of Tokyo, 1999.
[20] S.H. Chan, K.A. Khor, Z.T. Xia, J. Power Sources 93 (2001) 130–140.
[21] R.B. Bird, W.E. Stewart, E.N. Lightfoot, Transport Phenomena, Wiley, New York, 1960, p. 511.
[22] K. Kogaku (Ed.), Chemical Engineering Handbook, fifth ed., Kyokai, Maruzen Co. Ltd., Tokyo, 1994, p. 333 (in Japanese).
[23] E.R.G. Eckert, R.M. Drake Jr., Heat Mass Transfer, 1959.